Failure Modes of 3D-Printed Tessellated-Tile Beams

Grace F. Crocker, EIT, Sida Dai, Brandon E. Ross, PhD, PE, Michael Carlos Kleiss, PhD, Pinar Okumus, PhD, Negar Elhami-Khorasani, PhD, Seth Moore

¹Glenn Department of Civil Engineering, Clemson University, 110 Lowry Hall, Clemson, SC, 29631; Email: gfulmer@clemson.edu

²School of Architecture, Clemson University, Lee Hall, Clemson, SC 29634; Email: sidad@clemson.edu

³Glenn Department of Civil Engineering, Clemson University, 110 Lowry Hall, Clemson, SC, 29631; Email: bross2@clemson.edu

⁴School of Architecture, Clemson University, Lee Hall 3-123, Clemson, SC 29634; Email: crbh@clemson.edu

⁵Department of Civil, Structural and Environmental Engineering, University at Buffalo, 222 Ketter Hall, Buffalo, NY 14260; Email: pinaroku@buffalo.edu

⁶Department of Civil, Structural and Environmental Engineering, University at Buffalo, 136 Ketter Hall, Buffalo, NY 14260; Email: negarkho@buffalo.edu

⁷School of Architecture, Clemson University, Lee Hall, Clemson, SC 29634; Email: samr@clemson.edu

Abstract

Tessellations are patterns of repeating 2D geometric shapes that form an arrangement without gaps or overlaps. Although commonly used for their visual appeal in architecture, tessellations have only recently received attention for their applicability to structures as Tessellated Structural-Architectural (TeSA) systems. Because TeSA systems are composed of repeating discrete pieces (tiles), tessellated structural members have several potential benefits including, automated fabrication and construction, localization and repairability of structural damage, tunable structural behavior, and aesthetic value. This paper presents experiments in which small-scale (approximately 20 mm wide x 75 mm tall x 300 mm long) TeSA beams were fabricated from 3D printed tessellated tiles and then loaded to failure. Load-displacement response and failure mode are presented for six beam specimens, each having a different tessellated pattern. Stiffness, strength, and failure mode are compared between the different patterns. The results provide insights into how to design tessellated structures to achieve a desired structural response. While the notion of tessellated structures is still in its nascency, this paper introduces the concept, demonstrates and discusses its potential, and makes some critical observations about structural behavior and design.

Keywords: 3D printing, tessellated structures, failure modes, ductility

Introduction and Background

Tessellations are geometrically defined as repeating patterns of regular polygons forming an arrangement in one plane with no voids or overlaps. In architecture, tessellations are often utilized as an eye-catching aesthetic feature, such as the tiles in the Alhambra Palace in Granada, Spain. Some tessellated facades are used to control interior lighting and provide energy savings,

with few of these tessellated systems providing load resistance for the structure. Tessellated Structural-Architectural (TeSA) systems are structural systems that use tessellations in structural applications, such as load-bearing beams and shear walls, which are comprised of individual tiles arranged in a pattern. These TeSA systems provide the benefit of isolating damage to a few tiles which can then be replaced to rapidly repair the system. In addition to this resilient feature, a TeSA system can be considered a sustainable option due to its potential for disassembly, relocation, and reuse. Finally, TeSA systems are comprised of highly repetitive tiles; this characteristic makes TeSA systems conducive to automated fabrication and construction, as well as rapid transportation and on-site assembly (Ross et al. 2020).

The research presented in this paper is part of a larger project in which the numerical modeling and experimental testing of TeSA systems is being performed to investigate their mechanical properties. The TeSA concept lends itself well to creating systems of all scales; prior to the tests performed for this paper, tests have been performed on both medium-scale timber and medium-density fiberboard beams (Elsayed et al. in press) and a large-scale reinforced concrete shear wall (Crocker et al. 2021). Previous research by Estrin (2004) investigates the mechanical behavior of small-scale tessellated structures. The Estrin study was limited to the study of plates formed from small cubes. Due to the non-interlocking nature of the cubes, "edge boundaries" were required for these experiments to hold the plates together (much like buttressing in an arch). In contrast, the small-scale specimens discussed in this paper are designed to be topologically interlocking to mitigate the need for these edge boundaries.

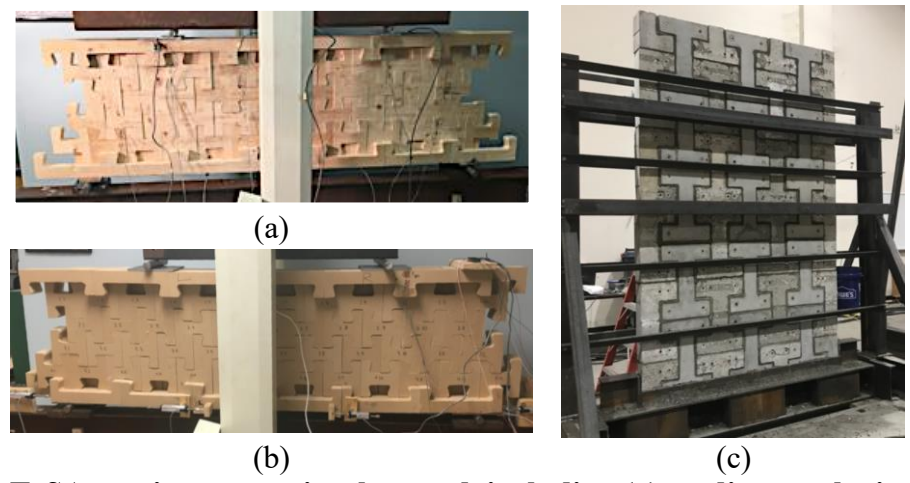


Figure 1: TeSA specimens previously tested, including (a) medium-scale timber beam (approximate span of 1.5 m), (b) medium-scale medium-density fiberboard beam (approximate span of 1.5 m), and (c) large-scale reinforced concrete shear wall (approximately 3 m tall).

This paper will describe the fabrication and testing of six small-scale 3D printed TeSA beams. This testing was performed to investigate the effects of different tessellated patterns and interlocking mechanisms on structural response. Small-scale 3D printed beams were designed to provide small, quickly manufactured specimens which could be tested to failure. In addition, fabricating these specimens on a small scale produces significantly less waste than testing numerous larger-scale specimens. In order to explore the differences in structural behavior based on the tessellated design, the different categories of tessellations must first be defined.

There are many types of tessellations, also referred to as "tilings," which can be categorized by the shapes of the polygons from which they are comprised. Regular tessellations are made up of a single identical regular convex polygon (Figure 2). There are three possible regular tessellations which are formed from triangles, squares, and hexagons. Semi-regular tessellations are formed by combining two or more regular convex polygons, and there are 8 possible types. There are also other types of tessellations such as demi-regular tessellations, but these types were not utilized in the design of the test specimens.

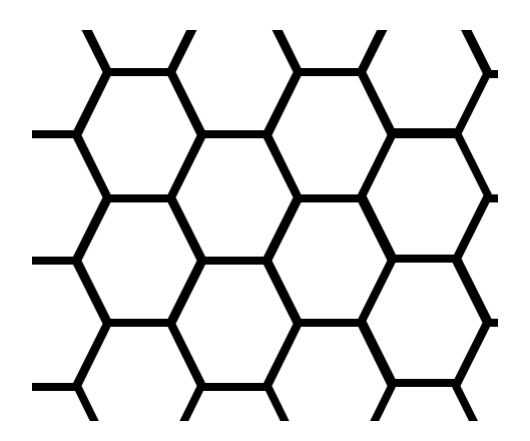


Figure 2: Example of a regular tessellation.

Specimen Design and Fabrication

Specimens were designed, fabricated, and tested in two groups: (1) the five original beam designs and (2) one "morphing" beam design. The first five beam specimens were drawn and modeled using Rhino 3D software, which can create and render curves, surfaces, and solids (Rhinoceros 3D 2021). Tiles and patterns were designed by the second author using the information in the previous section as inspiration for the designs. All of the patterns initially adhered to the strict definition of a tessellation and were comprised of non-interlocking convex shapes; after creating the patterns, the tiles were manipulated to create two-dimensionally interlocking mechanisms. In other words, the tiles were given interlocking "arms" which prevented translation vertically and horizontally (Figure 3). The beams were designed to have small gaps all around each tile as tolerances to make assembly easier.

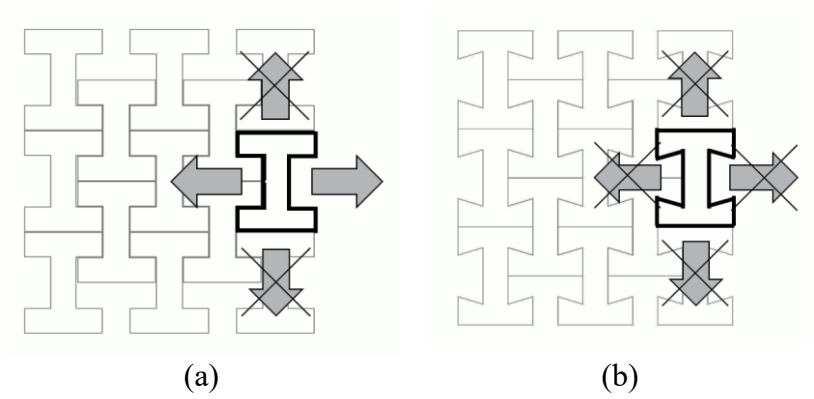


Figure 3: (a) Example of a one-dimensionally interlocking tessellation, (b) example of a two-dimensionally interlocking tessellation.

Once complete, the designs were printed using Polylactic Acid (PLA) filament (Figure 4). Infill with 100% density was used to produce solid tiles. Following printing, the individual tiles were arranged to construct the original five beam specimens, each of which was 304.8 mm long by 76.2 mm deep by 19.1 mm thick. The original five beam specimens can be seen in Figure 5. Alternating colors were used to help communicate the tiles designs; however, all tiles were built using the same type of filament.



Figure 4: (a) Digital model of tiles to be 3D printed, (b) photograph of printing process.

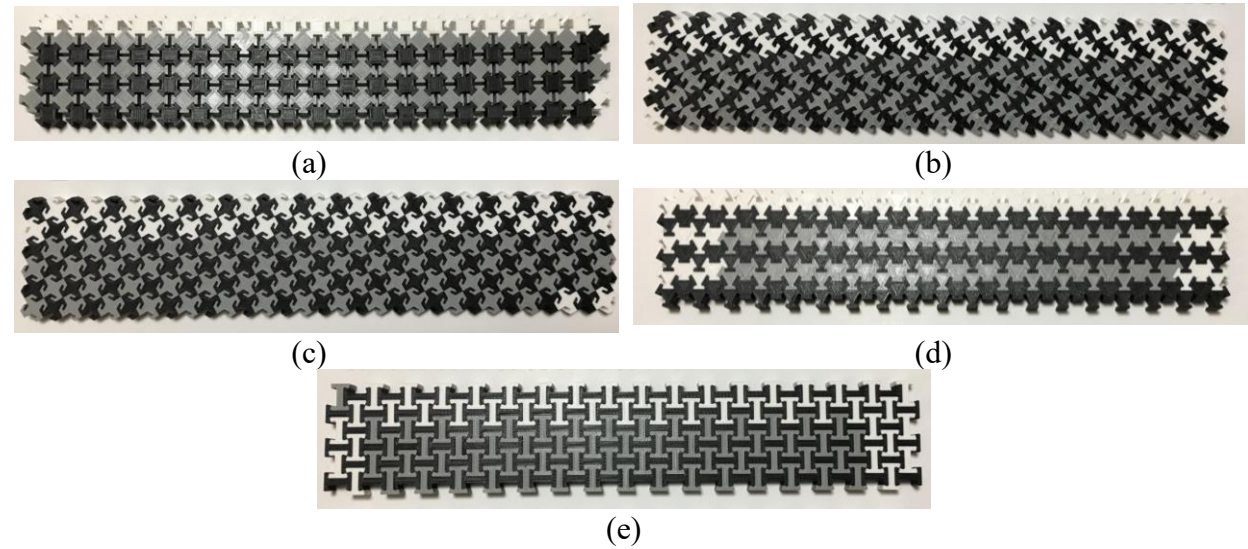


Figure 5: Photographs of fabricated original five beams: "A," "B," "C," "D," and "E."

Following testing and data analysis of the original five beams, a sixth "morphing" beam was designed, fabricated, and tested. This specimen will be referred to as the "morphing" beam and will be discussed separately as it utilized a different design methodology. A beam design system was developed to design this specimen using the Grasshopper software, a plugin for Rhino 3D which creates a visual programming environment, (Grasshopper 2021). A non-interlocking pattern was designed as before, and a two-dimensionally interlocking variation of the pattern was then generated by the Grasshopper system. Then, a "control curve" (shown in red in Figure 6) was developed which could be used to modify the key dimensions of the tiles. In doing this, the dimensions of the individual tiles were adjusted based on their distance and orientation relative to the control curve.

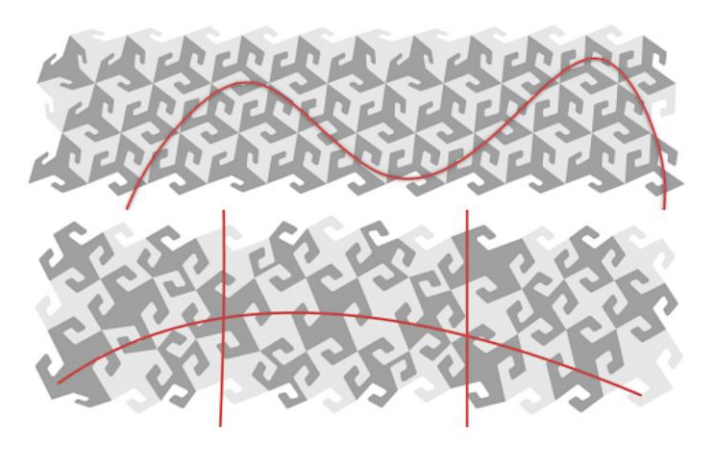


Figure 6: Examples of control curves being used to modify the tiles of the morphing beam using the Grasshopper system.

Once the tiles of the morphing beam were adjusted to practical dimensions for printing and testing, the design was again 3D printed using PLA. The tiles were subsequently assembled into the 298.5 mm long by 98.4 mm deep by 19.1 mm thick morphing beam specimen (Figure 7).



Figure 7: Photograph of fabricated morphing beam specimen.

Test Setup and Protocol

Once printed and assembled, the beam specimens were tested using a Universal Testing Machine (UTM). The specimens were simply supported by rollers, and a 76.2 mm wide diameter loading head was used to apply the load at the center of the beam (Figure 8). After testing the original five specimens, the decision was made to remove the loading head to apply the load to the morphing beam more precisely as a point load (Figure 9).

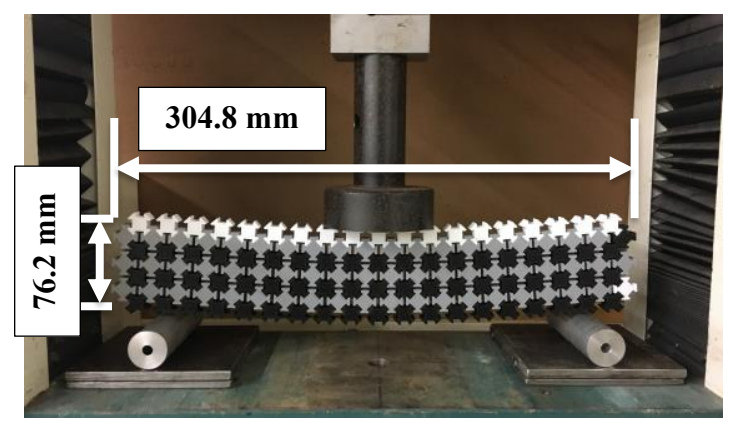


Figure 8: Example of test setup for original five beam specimens.

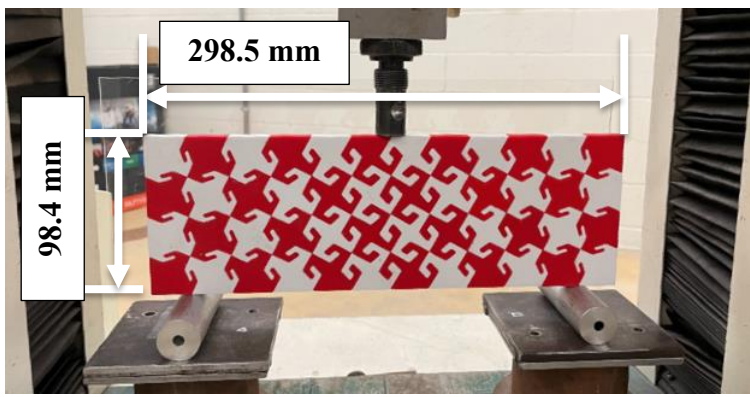


Figure 9: Test setup of morphing beam.

All specimens were tested using displacement-controlled protocols at a rate of 2.54 mm per second until complete failure was observed. For the first five beam specimens, the load was manually recorded from the UTM display every .254 mm of displacement. For the morphing beam specimen, the load was manually recorded from the UTM display every 1.27 mm of displacement. Out of plane movements were not observed to impact behavior of any of the specimens.

Results and Discussion

Original Designs

The peak applied load and displacement for the five original beam designs can be found in Table 1. Beam D showed the highest capacity (721 N), while Beam E had the lowest capacity (212 N). Beam B exhibited the greatest displacement (20.3 mm), while Beam D had the smallest displacement (10.4 mm).

Table 1: Summary of peak applied load and displacement values for 5 original beam specimens.

Beam Specimen	Peak Applied Load (N)	Peak Displacement (mm)
A	461	11.9
В	325	20.3
С	303	13.5
D	721	10.4
Е	212	17.8

The load-displacement responses of the five original TeSA beam specimens are shown in Figure 10. Beams tested in this experiment exhibited various responses which will be categorized as brittle, pseudo-ductile, or ductile. All of the beams experienced a degree of stiffening at the beginning of each test, which is attributed to closing of the gaps between tiles as loading commenced. Beams which exhibited brittle behavior have a load-displacement response characterized by nearly linear-elastic stiffness following gap-closure, then abrupt failure. Beams with pseudo-ductile behavior have load-displacement responses characterized by a period of

linear-elastic stiffness, yielding, then small stepwise failures until ultimate failure is reached. This type of failure will be referred to as "unzipping," which will be discussed in more detail later. Finally, beams associated with true ductile behavior are associated with load-displacement responses characterized by a period of linear-elastic stiffness, yielding, and fully plastic deformation before ultimate failure occurs. This behavior was caused by delamination of the PLA layers used to print the tiles.

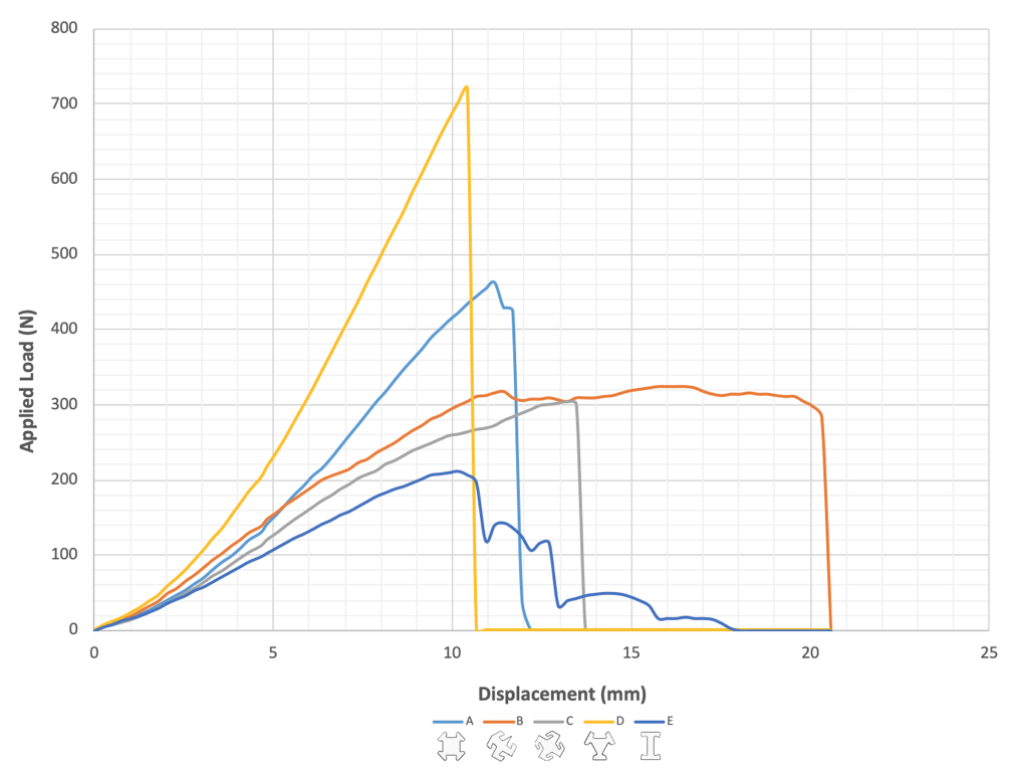


Figure 10: Load-displacement responses of original five TeSA beam specimens.

Beam A. Beam A is characterized by the small interlocking elements of its tiles. The load-displacement response of Beam A is shown in light blue in Figure 10. As discussed above, this beam experienced some initial stiffening during gap closure until approximately 100 N were applied. Thereafter, the specimen exhibited approximately linear-elastic behavior until about 300 N, when some slight softening became apparent as layers of PLA began to delaminate. The specimen continued to resist force until it experienced brittle failure at an applied load of approximately 461 N. At this moment, the PLA layers reached a level of deformation which allowed the tiles to "unsnap" from their initial interlocking position. The post-peak behavior was pseudo-ductile as the first unsnap event did not lead to total failure, but reduced the load to approximately 425 N. The subsequent unsnapping event led to failure as seen in Figure 11.

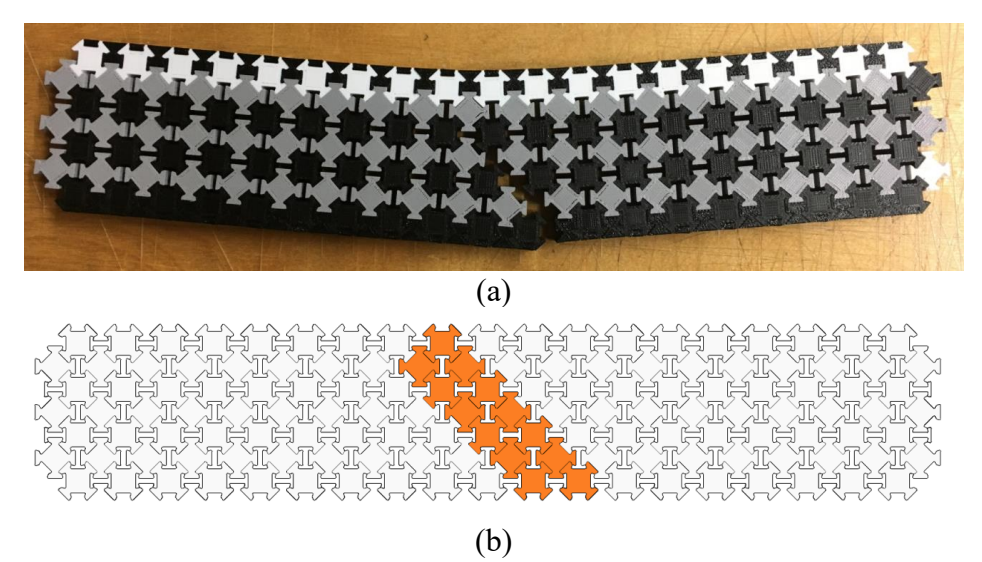


Figure 11: (a) Photograph of Beam A after testing, (b) highlighted failure path of Beam A.

Note that the "I" and "H" shapes are void spaces between the tiles.

Beam B. Specimen B is characterized by tiles with larger interlocking elements than Beam A. The load-displacement response of Beam B is shown in orange in Figure 10. This specimen exhibited a short period of approximately linear-elastic behavior (from about 50 N until about 200 N) after its initial stiffening. Softening began at this point when the PLA layers began to delaminate. The delamination continued, increasing rapidly around 320 N when the load-displacement response plateaued as the specimen continued to deform without resisting any more applied load. This specimen exhibited significantly more displacement before failure than any of the other five original designs. Finally, the specimen failed as the tiles at the beam center unsnapped or split as can be seen in Figure 12.

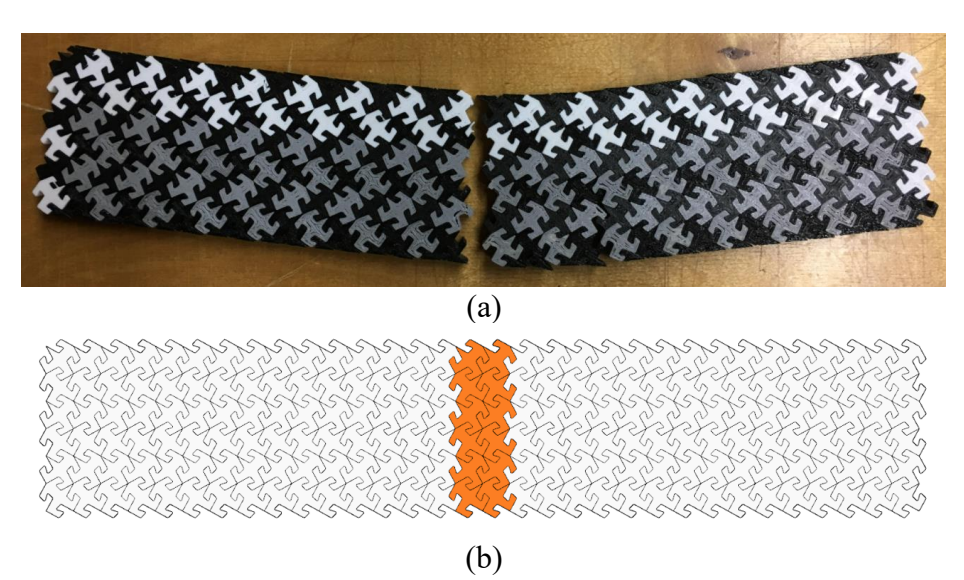


Figure 12: (a) Photograph of Beam B after testing, (b) highlighted failure path of Beam B.

Beam C. Beam C is characterized by its tiles with larger interlocking arms than Beam A, similar to Beam B. The load-displacement response of Beam C is shown in grey in Figure 10. Beam C completed its initial stiffening phase at around 50 N of applied load, then exhibited

approximately linear-elastic behavior until about 200 N. Thereafter, the specimen experienced gradual softening as the PLA layers began delaminating until the applied load reached about 303 N, at which time the specimen failed entirely. Although there were indications of softening, there was no distinct plateau, and the behavior is categorized as brittle. At peak load, a few of the interlocking arms detached from the tiles. The failure mechanism of Beam C is shown in Figure 13.

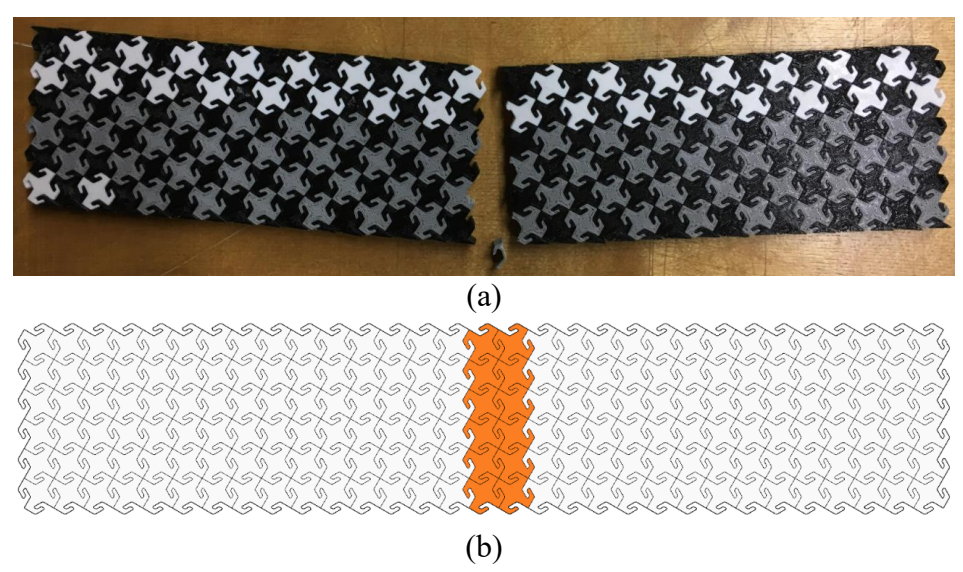


Figure 13: (a) Photograph of Beam C after testing, (b) highlighted failure path of Beam C.

Beam D. Much like Beam A, Beam D has tiles with small interlocking arms. The load-displacement response of Beam D is shown in yellow in Figure 10. This specimen exhibited stiffening until approximately 200 N of applied load. Thereafter, the stiffness of the specimen was approximately linear-elastic until an abrupt brittle failure at an applied load of approximately 721 N. This design had the highest strength of the five original specimens, but it was also the most brittle. Minimal PLA delamination occurred; in contrast to the other beams, failure occurred strictly due to the small interlocking arms snapping off or apart (Figure 14).

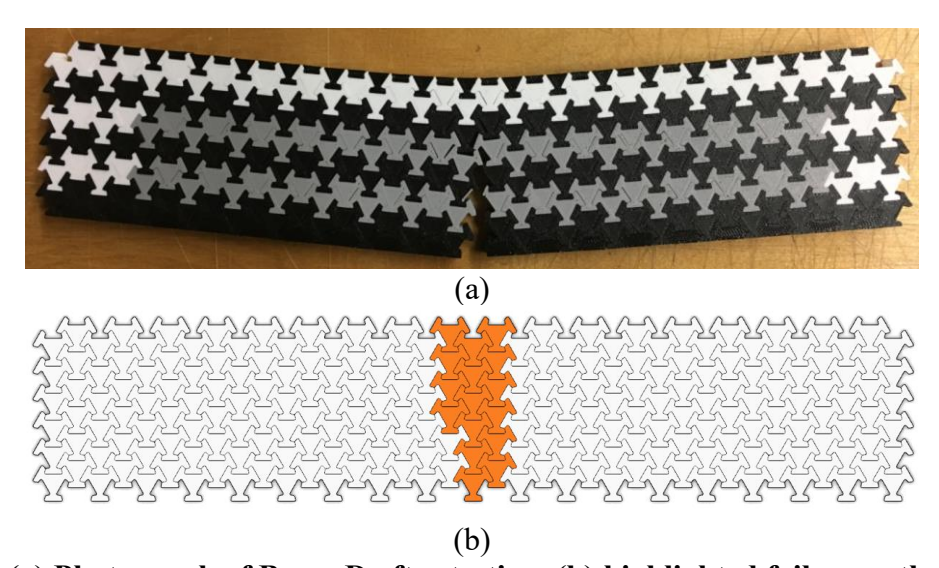


Figure 14: (a) Photograph of Beam D after testing, (b) highlighted failure path of Beam D.

Beam E. Like Beams A and D, Beam E also has tiles with small interlocking elements. However, Beam E is the only beam whose tiles have interlocking arms which are parallel to the loading direction. The unique load-displacement response of Beam E is shown in dark blue in Figure 10. This beam experienced the shortest period of initial stiffening of the five, with approximately linear elastic behavior starting around 20 N of applied load. Softening due to delamination began around 180 N. Shortly after this softening began, the interlocking arms of the tiles began snapping out of place without breaking. Each time an arm unsnapped, the specimen experienced a reduction in load resistance before stiffening again. This resulted in the "unzipping" pattern evident in Figure 10, which qualifies the behavior of Beam E as pseudoductile. The unzipping behavior can be attributed to the parallel orientation of the interlocking arms to the direction of the applied load, which prevents the small arms from failing in shear. The failure mechanism of this specimen can be seen in Figure 15.

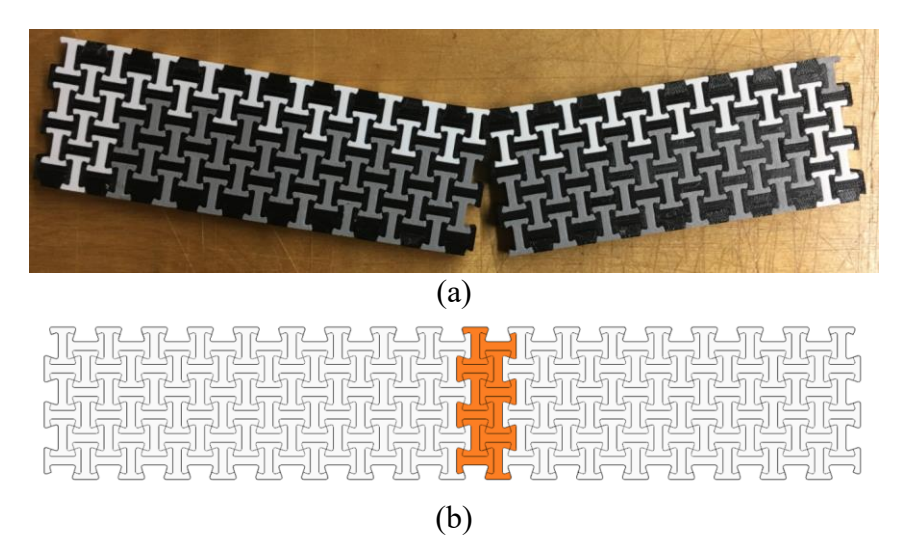


Figure 15: (a) Photograph of Beam E after testing, (b) highlighted failure path of Beam E.

Morphing Beam

The peak applied load resisted by the morphing beam was 395 N. The specimen experienced a peak displacement of 15.2 mm before failure. These results are summarized in Table 2.

Table 2: Summary of peak applied load and displacement of morphing beam.

Beam Specimen	Peak Applied Load (N)	Peak Displacement (mm)
Morphing	395	15.2

Figure 16 shows the load-displacement response of the morphing beam. Like the original designs, the morphing beam also exhibited an initial stiffening period until an applied load of about 85 N was reached. At this point, approximately linear-elastic behavior was observed until approximately 350 N of applied load. Softening then began due to delamination of the PLA and the associated bending of the interlocking arms out of their initial position. The peak applied load was approximately 395 N; the beam was highly ductile, continuing to soften and yield entirely before failing at an applied load of approximately 385 N. The failure was ultimately caused by the interlocking arms inelastically bending so far out of their initial position that they could no

longer support the load without completely delaminating or snapping off. The failure mechanism can be viewed in Figure 17.

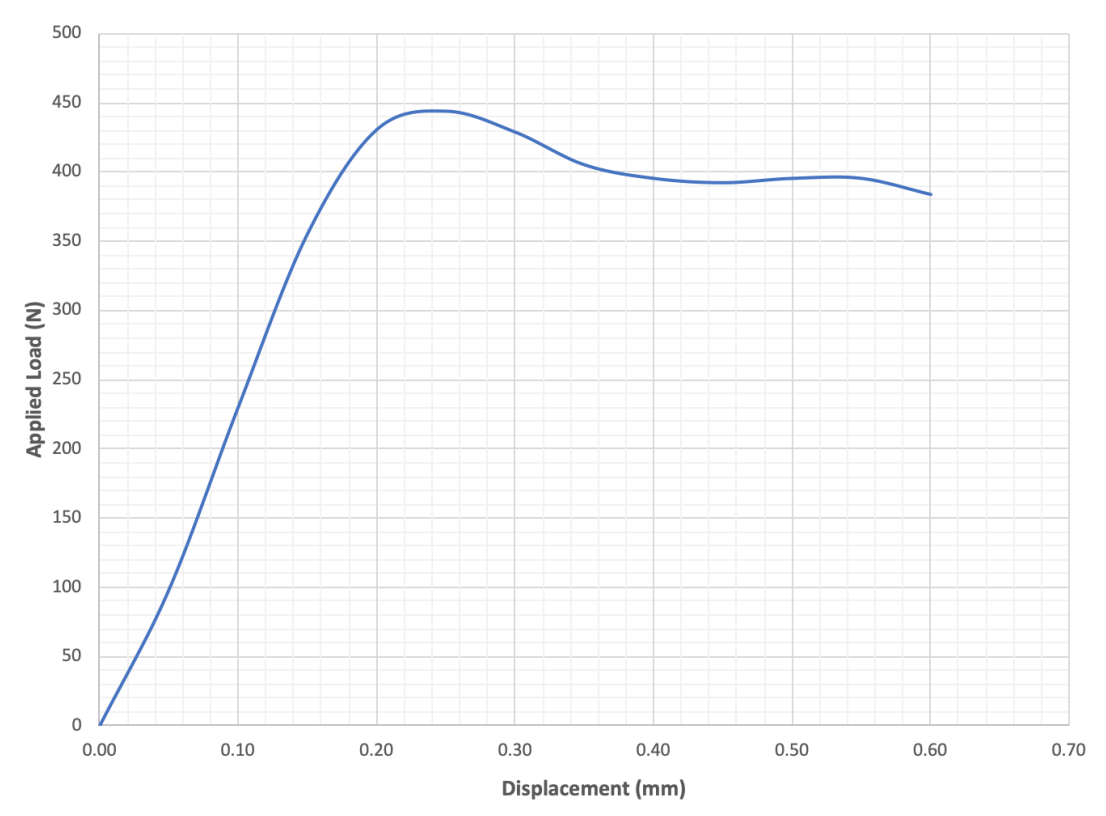


Figure 16: Load-displacement response of morphing beam.

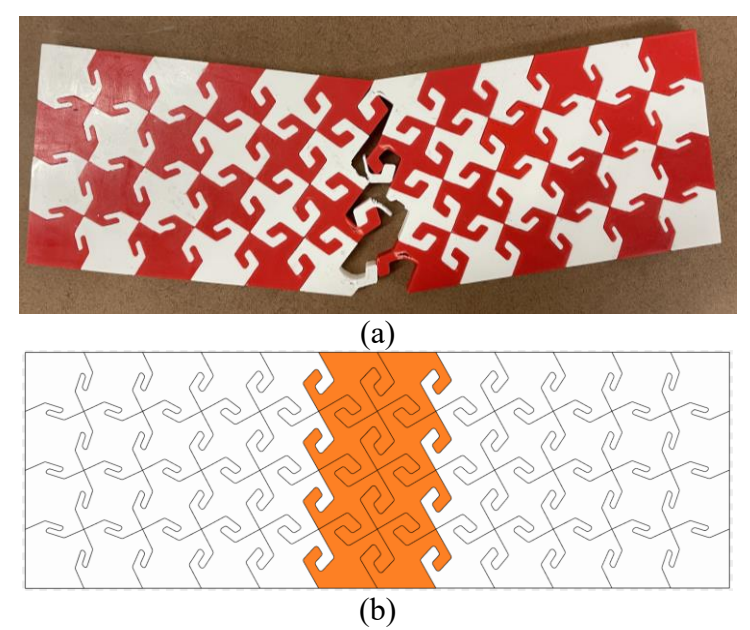


Figure 17: (a) Photograph of morphing beam after testing, (b) highlighted failure path of morphing beam.

Conclusions

Five TeSA beams were 3D printed and tested to failure to examine the effects of using different tessellated patterns on the load-displacement responses of the specimens. After the experiments, the lessons learned from developing and testing these beams were used to create a morphing beam design system in Grasshopper. This system was used to create a sixth beam that has morphing tiles, which was then tested in bending. This project yielded the following conclusions:

- Fabrication of small-scale beams through 3D printing and testing the beams with a UTM proved a valuable approach for exploring design ideas and evaluating structural behavior.
- The developed Grasshopper beam design system, which controls local variations on the tile geometry, provides a means for customizing tessellations based on the designers need. The control curves could potentially be used to optimize beams based on applied loads.
- Beams demonstrated three failure modes: brittle, pseudo-ductile, and ductile.
- This experiment helped identify some attributes which might contribute to a brittle failure and should therefore be avoided, such as the small interlocking arms used in Beams A and D. However, these small interlocking arms might be used strategically to cause pseudo-ductile failure, possibly by orienting them parallel to the applied loading direction, resulting in behavior like that of Beam E. In contrast, the larger interlocking arms of Beam B and the morphing beam allowed for ductile material behavior.
- In addition to affecting the failure behavior, the patterns also impacted strength and stiffness.

ACKNOWLEDGEMENTS

This material is based upon work supported by the National Science Foundation under Grant Nos. 1762899 and 1762133. Any opinions, findings, and conclusions or recommendations expressed in this material are those of the authors and do not necessarily reflect the views of the National Science Foundation.

Specimen fabrication and testing was supported by student Olivia Wright.

REFERENCES

- Associates, R. M. N. &. (n.d.). *Grasshopper new in Rhino 6*. www.rhino3d.com. Retrieved November 11, 2021, from https://www.rhino3d.com/6/new/grasshopper/.
- Associates, R. M. N. &. (n.d.). *Rhinoceros 3D*. www.rhino3d.com. Retrieved November 11, 2021, from https://www.rhino3d.com/.
- Crocker, G. F., Ross, B. E., Kleiss, M. C., Okumus, P., Khorasani, N. E., Romano J. M. (2021). "Design, Fabrication, and Assembly of a Tessellated Precast Concrete Shear Wall," *From the Proceedings of the 2021 PCI Convention, New Orleans, LA, May 2021.* Precast Concrete Institute.
- Elsayed, M. E. A., Crocker, G. F., Ross, B. E., Okumus, P., Kleiss, M. C., Khorasani, N. E. (in press). "Finite Element Modelling of Tessellated Beams," *Journal of Building Engineering*.

- Estrin, Y., Dyskin, A. V., Pasternak, E., Schaare, S., Stanchits, S., Kanel-Belov, A. J. (2004). Negative Stiffness of a Layer with Topologically Interlocked Elements. Scripta Materialia. 50(2), 291-294.
- Ross, B. E., Yang, C., Kleiss, M.C., Okumus, P., and Elhami Khorasani, N. (2020). "Tessellated Structural-Architectural Systems: Concept for Efficient Construction, Repair, and Disassembly," *Journal of Architectural Engineering*, v.26.